5-2023

An Investigation on the Effect of Conserved Hinge Histidine on Influenza Hemagglutinin(HA2) Protein Conformation Using MD Simulations

Nada Tolba

An Investigation on the Effect of Conserved Hinge Histidine on Influenza Hemagglutinin(HA2) Protein Conformation Using MD Simulations

An Honor's Thesis submitted for partial fulfillment of the requirements for honors studies in Chemistry and Biochemistry

By

Nada Tolba

Spring 2023
Chemistry and Biochemistry
Fulbright College of Arts and Sciences
University of Arkansas

Acknowledgements

I would like to thank Dr. Mahmoud Moradi for his support guidance, and mentorship over the course of this research investigation. I would like to also thank Shadi Badiee along with the rest of the Bimolecular Simulations Group for their continuous assistance over the progress of the investigation and analysis of this project. I would also like to recognize the Arkansas High Performance Computing Center(AHPCC) and the Texas Advanced Computing Center(TACC) for allowing me accessibility to the high-performance computing (HPC) and storage resources necessary for this investigation.

Table of Contents

I. Abstract

Hemagglutinin is a protein on the surface of Human Influenza Viruses.[1] It is composed of two glycopolypeptide domains, the HA1 and HA2 domains. Previous studies have found that across different strains of Influenza viruses, HIS435 residues remain conserved.[4] In studies where mutations occurred in hinge-site histadine residues, the Influenza virus was inactive.[4] These investigations indicated a significant role of HIS435 (hinge-site histadines) in virulence. Four systems were created using Molecular dynamics (MD) simulations. Each system was composed of an Isolated HA2 trimer solvated in a 150 mM NaCl rectangular water box at 310 K under isobaric and isothermal conditions . Conditions after endosomal acidification were simulated in two of the systems by protonating their HIS435 residues. Two systems remained with neutral HIS435 residues to simulate conditions before endosomal acidification. This experimental model was implemented to study the role of HIS435 on the mechanistic change in HA2 after endosomal acidification. The simulations were run for one microsecond. During this timeframe, all systems exhibited small-scale conformational changes, however a large-scale conformational change was not observed. This investigation is a continuation of previous research which had studied the microsecond-level conformational change of the full Hemagglutinin protein as it relates to pH and hinge histidine protonation states using molecular dynamics simulations.

II. Introduction

a. Supported mechanisms of HA2 Fusion

Hemagglutinin is a protein on the surface of Human Influenza Viruses.[1] It is composed of two glycopolypeptide domains, the HA1 and HA2 domains[2]. The HA1 domain is responsible for binding to sialic acid on the surface of host cells, allowing for viral entry into the host cell.[2] The HA2 domain is homotrimeric, consisting of three segments, "B," "D," and "F." Upon entering the host cell, the virus is still contained within an endosome. Following endosomal acidification, The HA2 domain has been found to undergo a series of large-scale conformational changes[1-2], allowing for the extension of a hydrophobic fusion peptide from the interior of the protein towards the host-cell membrane. This 20-30 residue peptide fuses the viral and endosomal membranes together, allowing viral RNA to be accessible to the host cell.[2-3,10,12]These mechanistic details which have been observed in preliminary studies are facilitated by a transition of B loops to alpha helices, allowing for the extension of the fusion peptide from the HA2 N-terminus towards the host cell membrane. The host and viral membranes are then able to fuse after a critical bending event at a hinge region of the HA2 peptides, supported by a helix to loop secondary structural transformation at the hinge region. [3,5,6-7] The hinge region is a 6-residue locale of the HA2 which has been found to be critical to the host cell-virion fusion event.[3]

b. Highly Conserved Histidine Residues

In recent studies, histidine residues have been targeted for research for their role in fusion activity for a multitude of reasons. Previous studies have found that across different strains of Influenza viruses, Histidine residues in the hinge region of the HA2 glycoprotein have been found to be highly conserved across Influenza hemagglutinin subtypes.[3,4] Additionally, Histidine contains an imidazole functional group which has a pKa that overlaps with the pH range of the endosome. Histidine is the only HA residue with a pKa corresponding to acidified endosomal pH values.[3] Both the highly conserved status of histidine residues and its pKa indicate a role in pH-dependent conformational changes of HA. Another indicator of the significance of hinge histidine residues is the fact that in studies where mutations were introduced to the highly conserved hinge histidine sites of HA2, membrane fusion activity was not exhibited[3,4] thereby inhibiting viral RNA from being accessible to the host cell. In a study where the hinge histidine

was mutated to Alanine, hinge-site bending activity was not observed.[3] These investigations indicated a significant role of HIS435 in virulence.

c. Past and Current Investigative Templates

This investigation is an extension of preliminary studies in the UARK Biomolecular Simulations lab which simulated the effects of HIS106 protonation states on the global transmembrane HA protein configuration dynamic in order to investigate the effects of hinge histidine protonation on the HA protein and its fusion mechanism. These preliminary studies indicated a distancing of the HA1 domains of the HA protein during a 2.4 μs time frame, which is a change that is expected in the active Endosomal HA protein under physiological conditions.[9] This investigation aims to analyze the configuration of only the isolated HA2 segments. HIS106 will be referred to as HIS435 in correspondence with its position in the isolated HA2 models.

All atom equilibrium Molecular dynamics simulations were preformed to investigate the role of HIS435 on the configuration dynamic and fusion mechanism of isolated HA2 trimers. Four systems were created. Each system was composed of an Isolated HA2 trimer solvated in a 150.0mM NaCl water box at 310 K under isobaric and isothermal conditions to simulate physiological conditions. At a pH between 6 and 9.3, HIS exists in its neutral form[13] (HSD), thus two systems consisting of the HIS435 zwitterions were created to model the states of the HIS435 residues before endosomal acidification at physiological pH. At a pH level between 1.8 and 6, HIS exists in a positively charged state with a charged imidazole and amide group.[13] Considering this, The next two systems consisted of the positively charged HIS435 (HSP435) residues, simulating conditions after endosomal acidification. We are expecting to observe some of the major conformational changes discussed in part A which are hallmarks of HA fusion in the protonated systems (3P) as opposed to the non-protonated systems (0P).

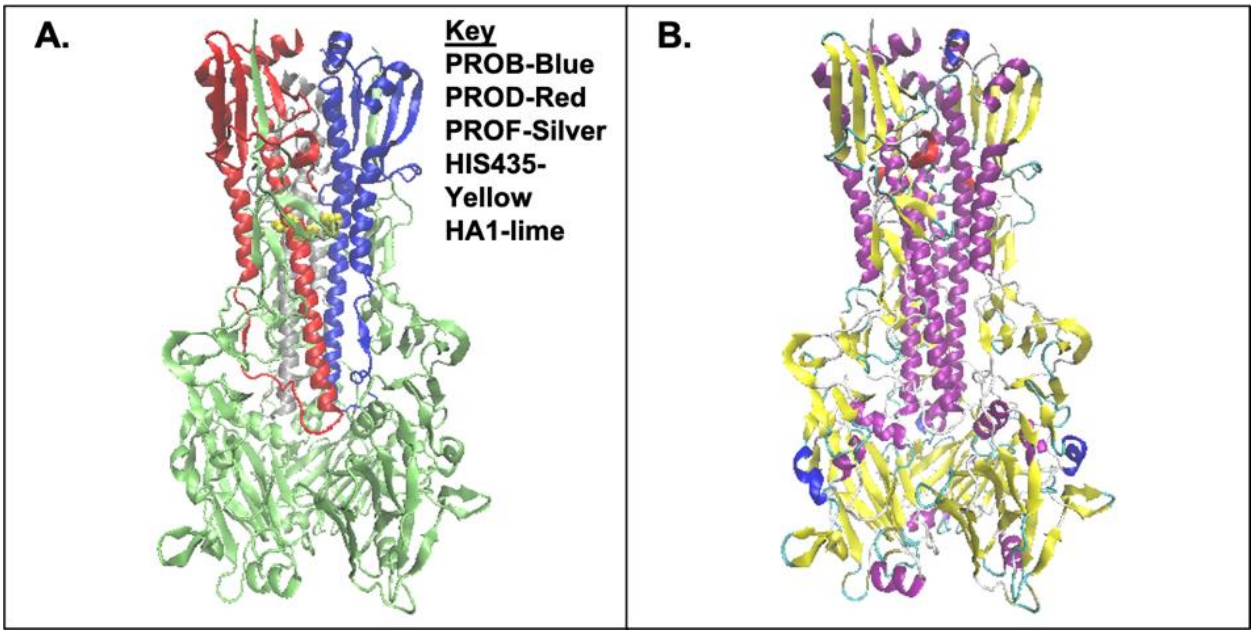

Figure 1. Part A. displays each monomer of HA2, PROB, PROD, and PROF, HA1 and the protonated hinge histidines. The monomers were visualized using the VMD ColorID coloring method and the New Cartoon drawing method. The Histidines were visualized usingt the ColorID coloring method and the VDW drawing method. Part B. is a visualization of the HA glycoprotein using the New Cartoon drawing method and the secondary structure coloring method to clearly depict alpha helices, beta sheets and loops.

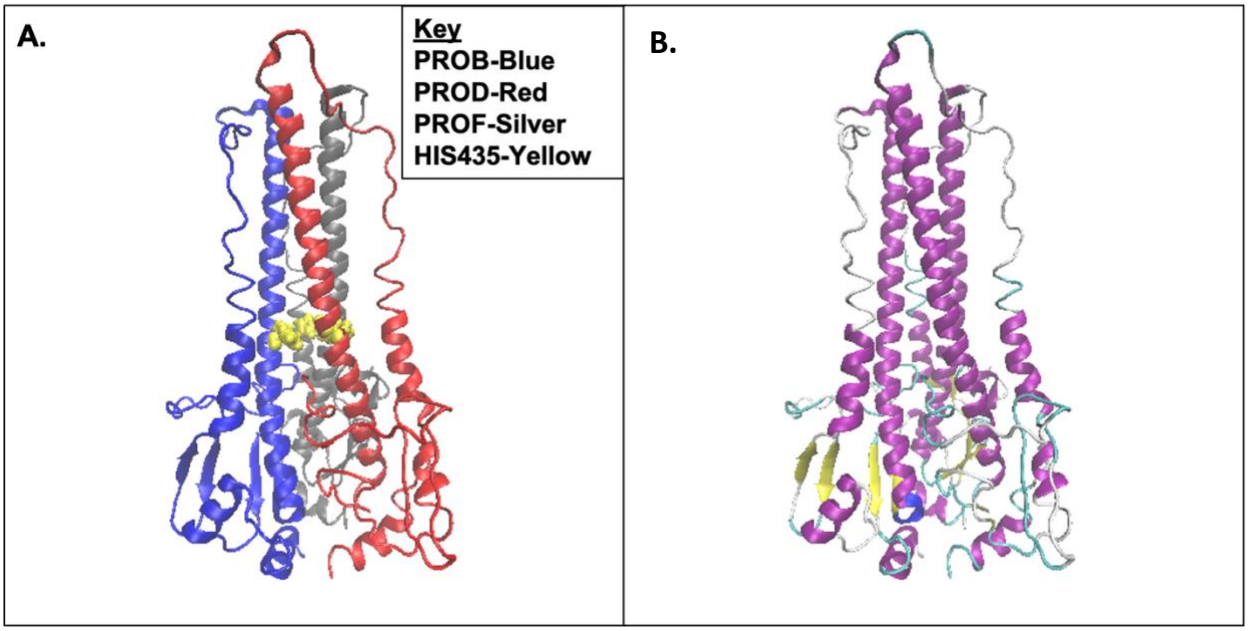

Figure 2. Part A. displays each monomer of HA2, PROB, PROD, and PROF, as well as the protonated hinge histidines. The monomers were visualized using the VMD ColorID coloring method and the New Cartoon drawing method. The Histidines were visualized usingt the ColorID coloring method and the VDW drawing method. Part B. is a visualization of the HA2 glycoprotein using the New Cartoon drawing method and the secondary structure coloring method to clearly depict alpha helices, beta sheets and loops.

III. Methods

The X-ray crystal structure of the HA2 Influenza Hemagglutinin glycoprotein was obtained using the Protein Data Bank (PDB file: 5KUY for type H3 type A Influenza Hemagglutinin, H3N2).[8] The CHARMM_GUII Input Generator [14,18,19,25] was then utilized to set the force fields and create the models critical to this investigation. Four systems were created using All atom (AA) microsecond-level Molecular Dynamics (MD) simulations. Two of these systems consisted of a protonated triplet set of HIS435 (HSP 435) residues on each segment of the HA2 homotrimer, emulating the state of HIS435 under acidic endosomal conditions(pH ~6).[3] The next two systems consisted of a triplet set of the zwitterionic form of HIS435 (HSD 435), emulating the state of HIS435 under physiological pH conditions. Each system was solvated in a 150 mM NaCl water box and maintained under isothermal and isobaric conditions(NPT ensemble) at 310K and 1 atm. All models consisted of approximately 237700 atoms and simulations were run through NAMD using a 2.0 fs time step. Systems were first equilibrated. The particle Mesh Ewald method (PME) was the algorithm incorporated into the parameters set for this investigation. A PME grid spacing of 1.0 and a PME interpolation order of 6 were applied. Periodic boundary conditions were implemented.[20] Constant temperature was maintained through Langevin dynamics with a damping coefficient of 1/ps.[20]

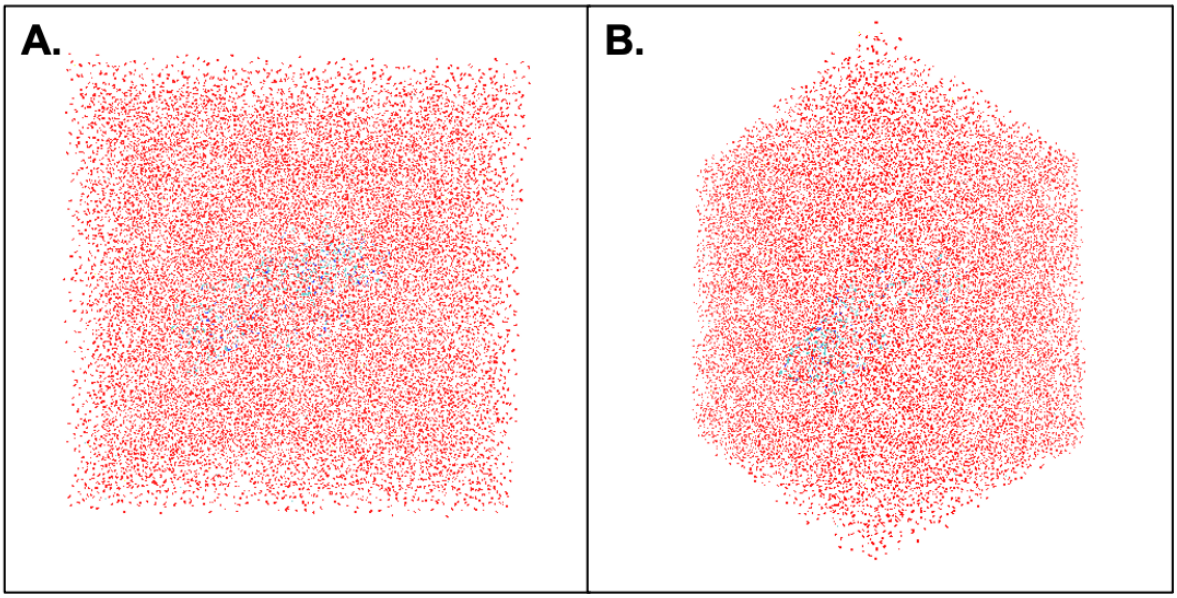

Figure 3. A vizualization of the water box constructed to encompass the HA2 structure. Water moleculles are depicted in red and the HA2 glycoprotein is depicted in blue. The VMD lines drawing method and names coloring method were utilized to create these renderings. Figure 2A. is a front-facing view of the water box and Figure 2B. is a side-facing view.

Preliminary simulations were each 1 us long, accounting for a cumulative 4 us simulation length. The computing capacity of the University of Arkansas High Performance Computing Center (AHPC) Pinnacle and Trestles Supercomputers was utilized to perform the simulations investigated here. The computational capacity of the Texas Advanced Computing Center (TACC) was also utilized. Each job submission produced a nanosecond-scale increase in the simulation time. The individual dcd files for each model were subsequently concatenated, resulting in four 26-27 GB dcd files, each containing the cumulative microsecond simulation length for its respective system. The dcd files were loaded into the VMD Interface along with the relevant psf file for each system. Due to limitations on storage capacity during the time of this investigation, a stride of 20 was used in the loading process to condense the files to be more manageable for analysis. The VMD interface was utilized for protein visualization and analysis. An analysis of the Root Mean Square Deviation (RMSD) , Root Mean Square Fluctuation (RMSF) , Salt Bridges, Hydrogen Bonds, and angles were all preformed to quantize the configuration dynamic across all four systems. RMSD, RMSF, and Salt Bridge measurements, obtained via the VMD software were then visualized using the graphing capabilities of gnuplot.

IV. Results and Discussion

a. Trajectories

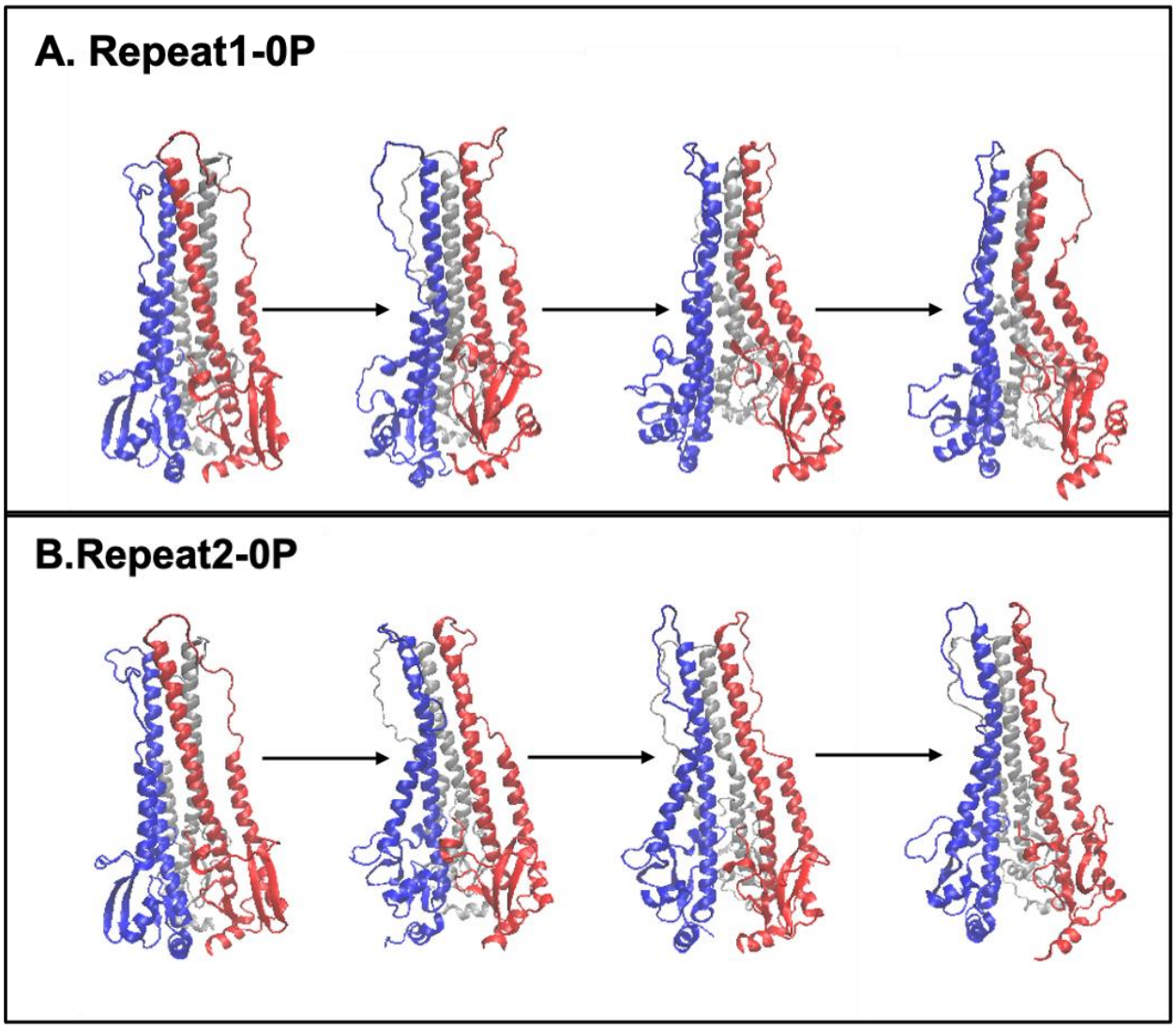

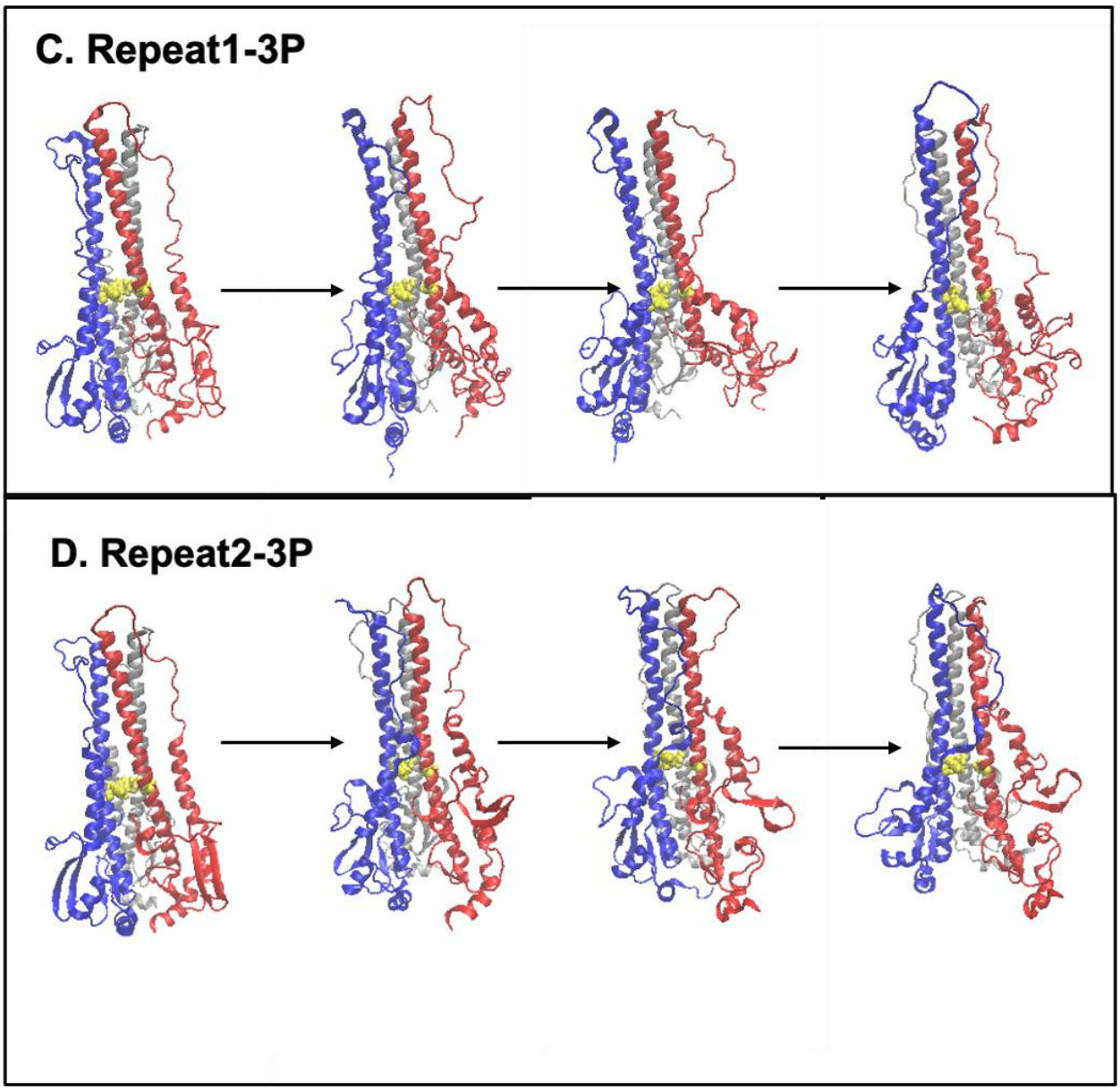

Figure 4. Parts A and B depict the trajectories of the non-protonated repeats. The leftmost HA2 visualizations are the HA2 glycoproteins at 0 us. The rightmost visualizations are the HA2 glycoproteins at 1 us. Parts C and D depict the protonated HA2 glycoproteins. Like Parts A and D, the leftmost HA2 visualizations are the HA2 glycoproteins at 0 us. The rightmost visualizations are the HA2 glycoproteins at 1 μs. Parts A and D each capture the middle segments after 300 ns and 600 ns, respectively. Parts B and C capture the middle segments after 312 ns and 520 ns, respectively.

Based on the trajectory visualization, all models appeared to experience distancing of their segments at the C-terminus, regardless of protonation state**(Figure 4)**. Based on previous studies, expansion has been found to allow for the HA2 glycoprotein to span the viral membrane, a key step in the process of viral-host cell membrane fusion.[21] Interestingly, the lack of

protonation of the HIS435 in the hinge region does not visibly inhibit segment distancing at the C-terminus. These trajectories do not indicate the full range of the large-scale conformational changes expected based on previous investigations. Within the short 1 us simulation period, we did not observe large-scale helix to loop conformational changes or loop to helix conformational changes as is expected based on previous studies of HA2 fusion. Subsequently, an extended HA2 helical structure was not observed.[22,23] It is possible that more simulation time is necessary to better encapsulate the full range of the HA2 configuration dynamic.

b. Root Mean Square Deviation (RMSD) Analysis

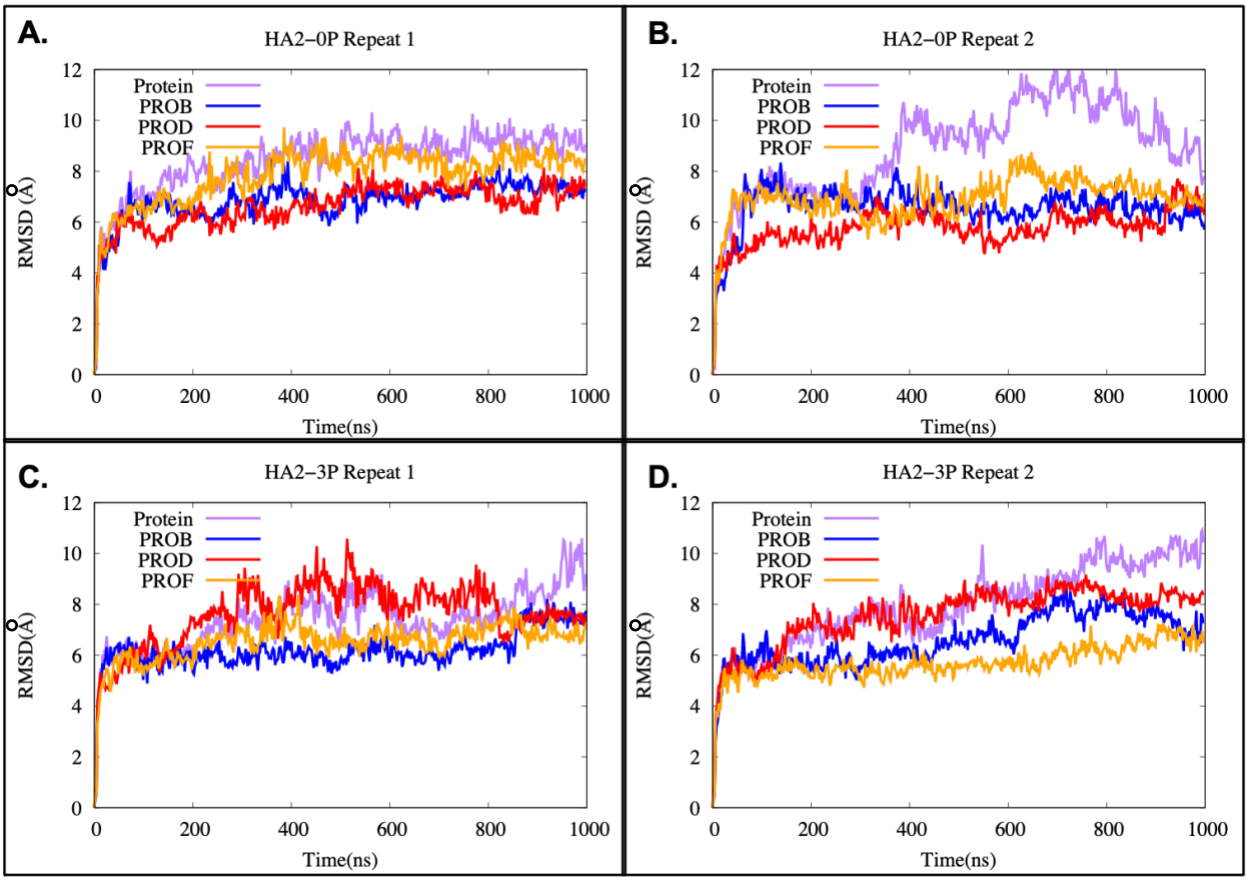

Figure 5. Overall RMSD for the HA2 protein and each HA2 segment for protonated (3P) and non-protonated repeats(0P), measured in reference to the alpha carbon(C_α) backbone.

Root Mean Square Deviation(RMSD) Calculations were utilized to quantify the change in position of the alpha Carbon backbone (C_α) of the protein in reference to the original coordinates at 0 us over the 1 us simulation time frame. In both non-protonated repeat models, the overall protein RMSD increases to beyond ten angstroms at a point between 300 and 600 ns, then can be

observed decreasing below 10 A by the end of the one microsecond time frame. Overall protein RMSD plots for both 0P models exhibit an overall negative slope at the end of the 1 us time frame (800-1000 ns) ; conversely, the protonated repeat models exhibit an overall positive protein RMSD after 700 ns that increases to a value beyond 10 Å near the end of the 1 μs time-frame. The 0P and 3P models diverge in the signs of their overall slopes for the overall protein RMSD in the 800-1000 ns time-frame at the terminal of the simulation period. More simulation time is necessary to fully evaluate the RMSD of the 0P repeats, in comparison to the 3P repeats. Along with overall protein RMSD, internal RMSD was calculated for the HA2 monomers. The internal RMSD values do not indicate a large-scale conformation change within the 1 μs time-frame.

c. Root Mean Square Fluctuation (RMSF) Analysis

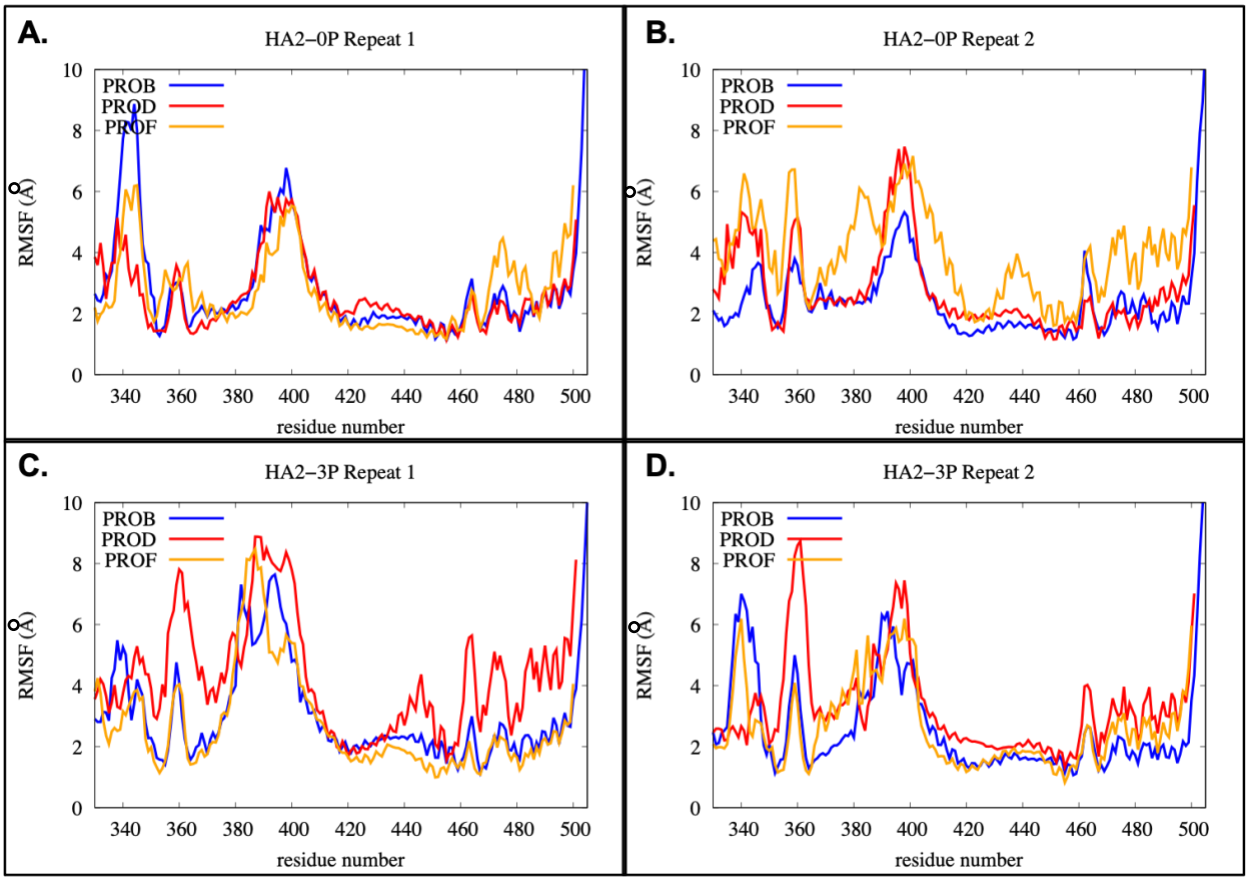

Figure 6. RMSF for each residue on each monomer of HA2 over a 1 us simulation period is depicted above for 0P systems 1 and 2 (A and B, respectively) and 3P systems 1 and 2 (C and D, respectively)

Root Mean Square Fluctuation(RMSF) calculations were utilized to quantify the average change in position of each residue over the course of the one microsecond simulation period. Each monomer is comprised of an approximate range of 330-505 residues as depicted in **Figure 6**. The RMSF plots do not suggest a consistent discernable pattern between the dynamic of the residues in 0P as opposed to 3P systems.

d. H-bond Occupancy Data

H-bond	0P-Repeat 1	0P-Repeat 2	3P-Repeat 1	3P-Repeat 2	Average 0P	Average 3P
HIS435-Side ASP438-Side	**1.59%**	**3.72%**	**46.69%**	**61.16%**	**2.66%**	**53.93%**
ASN382-Main ASN378-Main	**60.16%**	**59.30%**	**7.64%**	**7.37%**	**59.73**	**7.51%**
LYS387-Side GLU426-Side	**16.14%**	**14.46%**	**26.65%**	**59.76%**	**15.3%**	**43.21%**

Table 1. A comparison of H-bonds across 0P and 3P systems. H-bonds involving main *atoms* can involve amino or carboxyl groups. H-bonds between *side* chains involve R-groups.

H-bonds have been found to add to the stability of a protein structure.[17] The first and second 0P systems exhibited a total of 1071 and 1110 hydrogen bonds, respectively. The first and second 3P systems exhibited a total of 1148 and 1105 hydrogen bonds respectively. The 0P systems exhibited a mean of 1091 H-bonds. The 3P models exhibited a mean of 1127. The cutoff distance for H-bond calculation was 3.0 Å and the angle cutoff was 20 degrees. The 0P systems exhibited an average H-bond occupancy of 2.66% for the HIS435 side-ASP438 side bond, which

is twenty times less than the average H-bond occupancy of the HIS435 side-ASP438 side bond for the 3P system. By evaluating discrepancies in H-bond occupancy levels between the models, localized conformational differences can be discovered.

The 0P systems exhibited an average H-bond occupancy of 59.73% for the ASN382 Main -ASN378 Main bond, which is eight times greater than the average H-bond occupancy of the corresponding bond for the 3P system.

The 0P systems exhibited an average H-bond occupancy of 15.3% for the LYS387-Side GLU426-Side bond, which is three times less than the average H-bond occupancy of the corresponding bond for the 3P system.

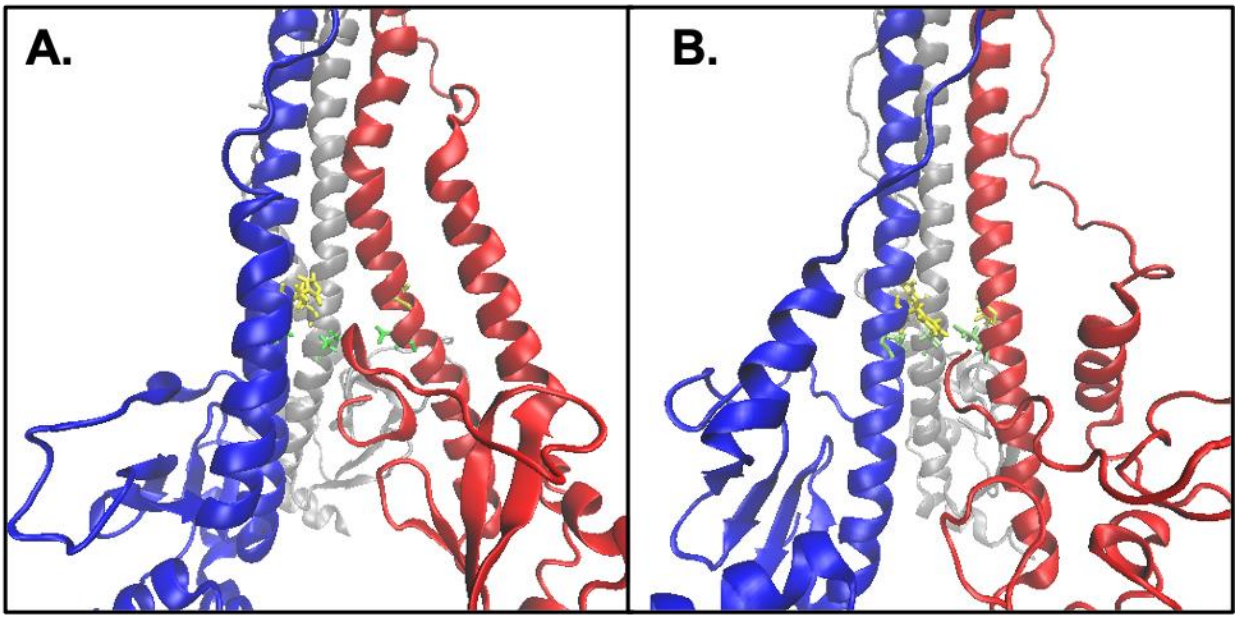

Figure 7. The rendering depicted above displays HIS435 residues (yellow) ASP438 (green) after 1 *us* simulation time in the 0P-repeat 1(A) and 3P-Repeat 1(B).

The interaction between the HIS435 Imidazole ring side chain and the ASP438 carboxylic acid side chain exhibited an average H-bond occupancy in the 3P repeats 20 times as large as that of the 0P repeats **(Table 1),** meaning the H-bonds between these side chains are more resilient and ever-present throughout the length of the 3P simulation than in the 0P simulations. The implication of this finding is that in the 3P models, the segments are closer together at the hinge region than in the 0P models. In the trajectory models **(Figure 4),** the 3P models sometimes appear "pinched" at the hinge region, in comparison to the 0P models. This is

likely partially attributable to the higher H-bond occupancy between the hinge HIS435 and ASP438.

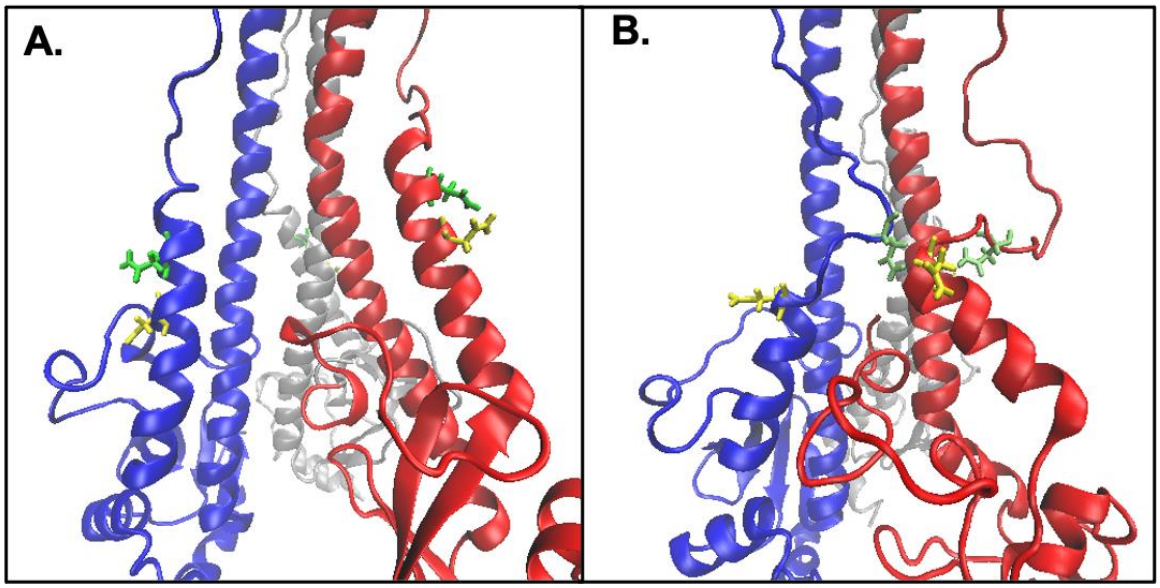

Figure 8. The rendering depicted above displays ASN382 residues(lime) and ASN378 (yellow) after 680 ns and 604 ns simulation time in the 0P-repeat 1 (A) and 3P-Repeat 1 (B), respectively.

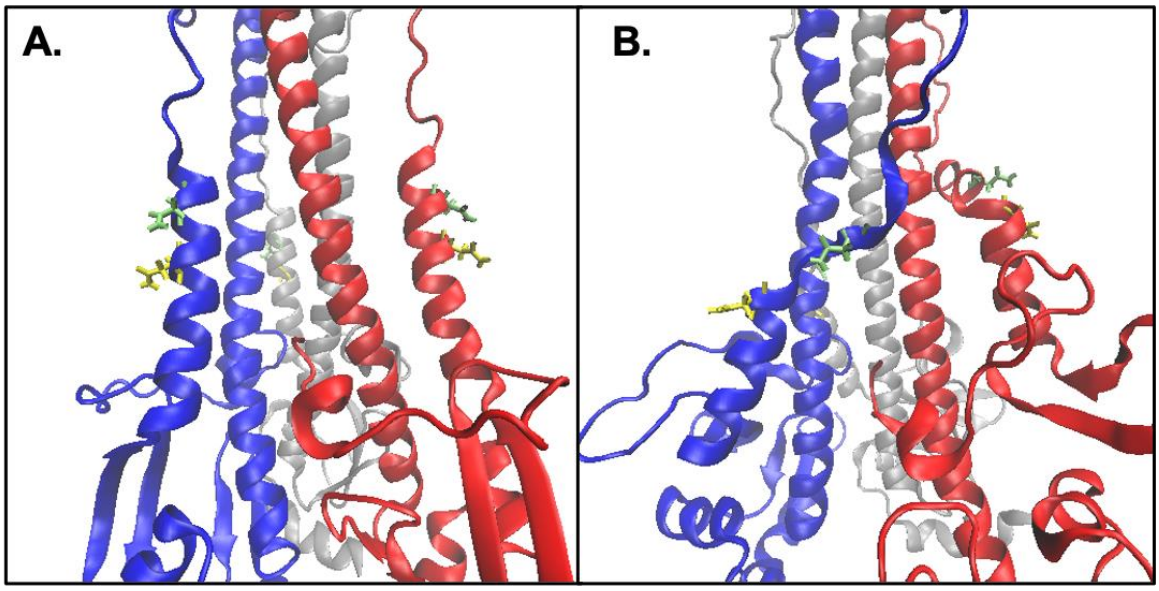

Figure 9. The rendering depicted above displays ASN382 residues (lime) and ASN378 (yellow) after 0 ns (A) and 1000 ns (B) simulation time in 3P-repeat 2.

The H-bond occupancy difference seen here**(Table 1 and Figure 9)** can be attributed to differences in secondary structure. The 0P repeats exhibit high H-bond occupancy between the main chains of ASN-382 and ASN378 because their locales remain coiled, so the distance between the small distance between the residues is conducive to H-bond formation. In 3P-Repeat 1, however, the residues reside on loops in the secondary structure of the protein, resulting in a larger distance separation for a large part of the simulation in comparison to the 0P models. In 3P repeat 2, the helices containing the residues begin to uncoil **(Figure 9B),** therefore increasing distance between them and decreasing H-bond occupancy between the relevant residues during the simulation.

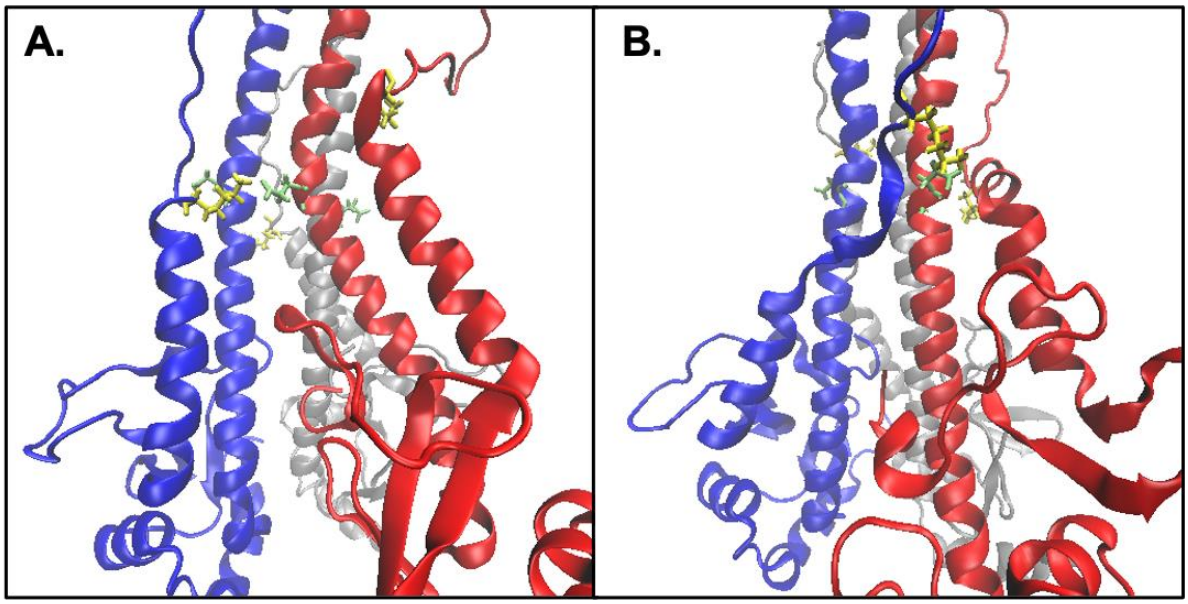

Figure 10. The rendering depicted above displays LYS 387 residues (yellow) and GLU426 (lime) after 1000 ns in 0P-repeat 1 (A) and 3P-repeat 2 (B).

Glu426 is a residue that is proximal to the hinge Histidine of interest in this investigation. It lies on helical segments of the HA2 structure, whereas the LYS 387 residues reside on looped structures. Thus, interactions between side chains of these residues usually result in a shorter loop to helix distance at the residue locales as shown in **Figure 10B**.

e. **Salt Bridges**

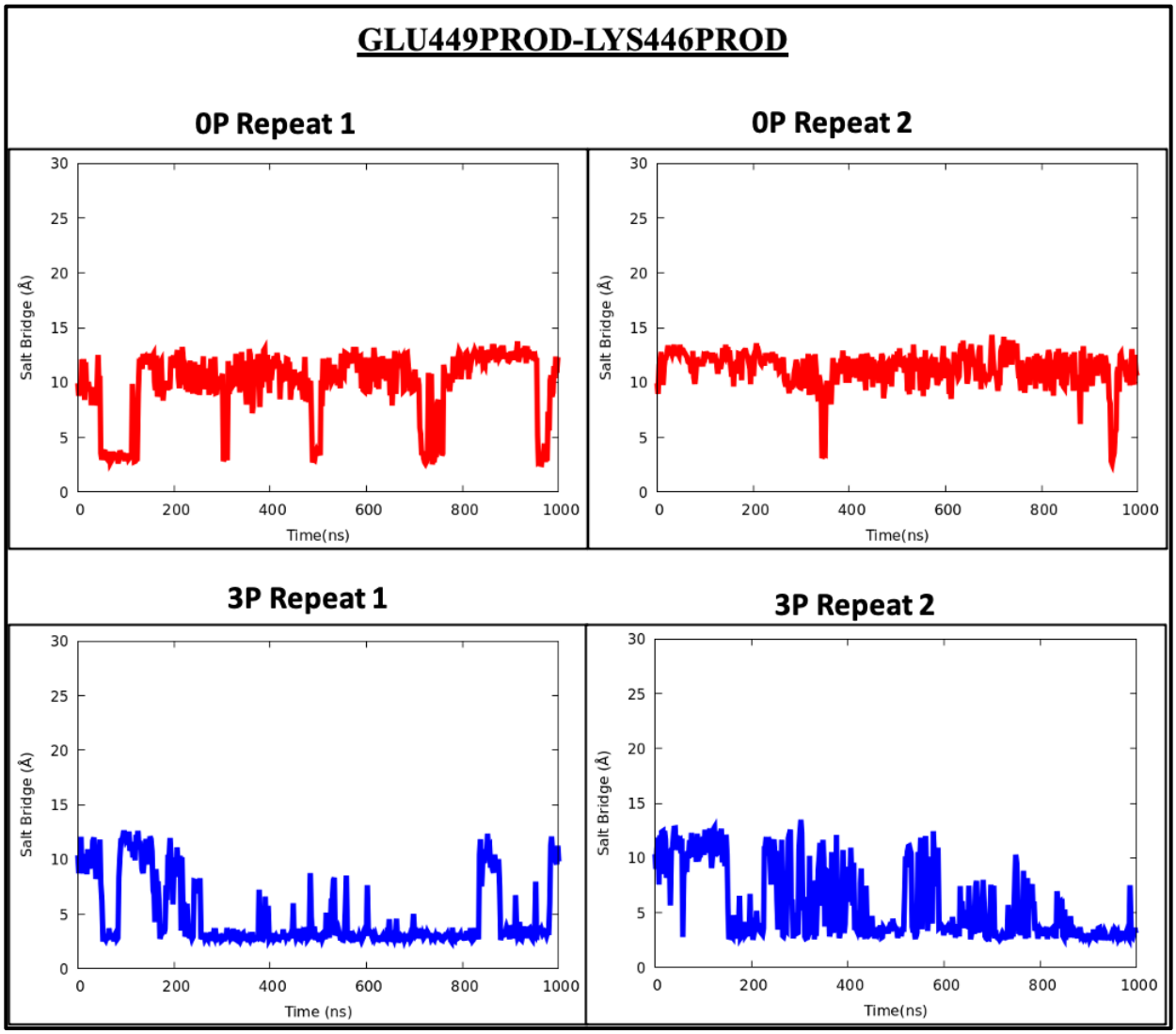

Figure 11. Salt Bridge dynamic between residues Glu449 PROD LYS446 on segment PROD over the 1.0 μs time frame is depicted above for 0P and 3P repeats.

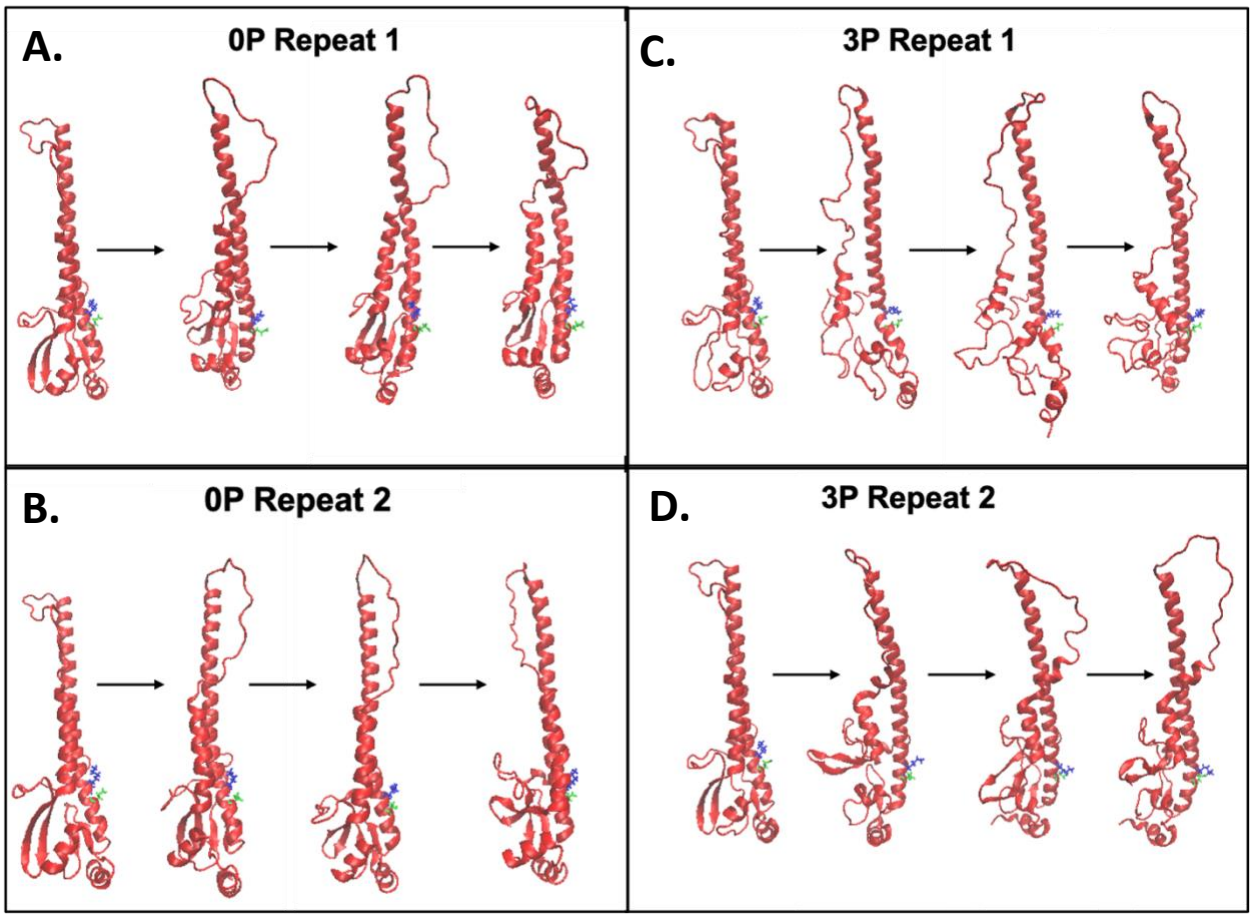

Figure 12. Glu449 (green residue) on segment PROD and LYS446 (blue residue) on segment PROD are depicted above for all repeats. The leftmost visualizations occur at 0 μs. The rightmost visualizations are the HA2 glycoproteins occur at 1 μs. Parts A and D each capture the middle segments after 300 ns and 600 ns, respectively. Parts B and C capture the middle segments after 312 ns and 520 ns, respectively.

Salt Bridges are ionic interactions between acidic and basic residues which can have a stabilizing effect on proteins[15,16]. By identifying differences in the dynamics and formation of salt bridges along the HA2 glycoprotein during the simulation timeframe, details of the HA2 configuration dynamic can be uncovered. A Nitrogen-Oxygen distance of 3.2 Å or less was used to indicate the presence of salt-bridges. As depicted in **Figure 11**, a salt bridge was observed between Glu449 PROD and LYS446 PROD for a larger range the simulation time for the 3P repeats in contrast to the 0P repeats. The 3P repeats both exhibited a Glu449PROD and LYS446 PROD salt bridge after 200 ns which broke and reformed variably during the remainder of the simulation period. Visualization of the 0P and 3P PROD segments **(Figure 12)** over the simulation period reveals that the bending activity of the PROD segments influences salt bridge formation. This bending is

likely what is conducive to the salt bridge formations observed as it decreases the distance between the charged groups on the residues to a value below 3.2 A. It should be noted that the residues participating in this salt bridge are proximal to the hinge histidine of interest in this investigation. We know from previous studies that changes in the hinge histidine are likely to influence behavior of proximal regions.[4,24]

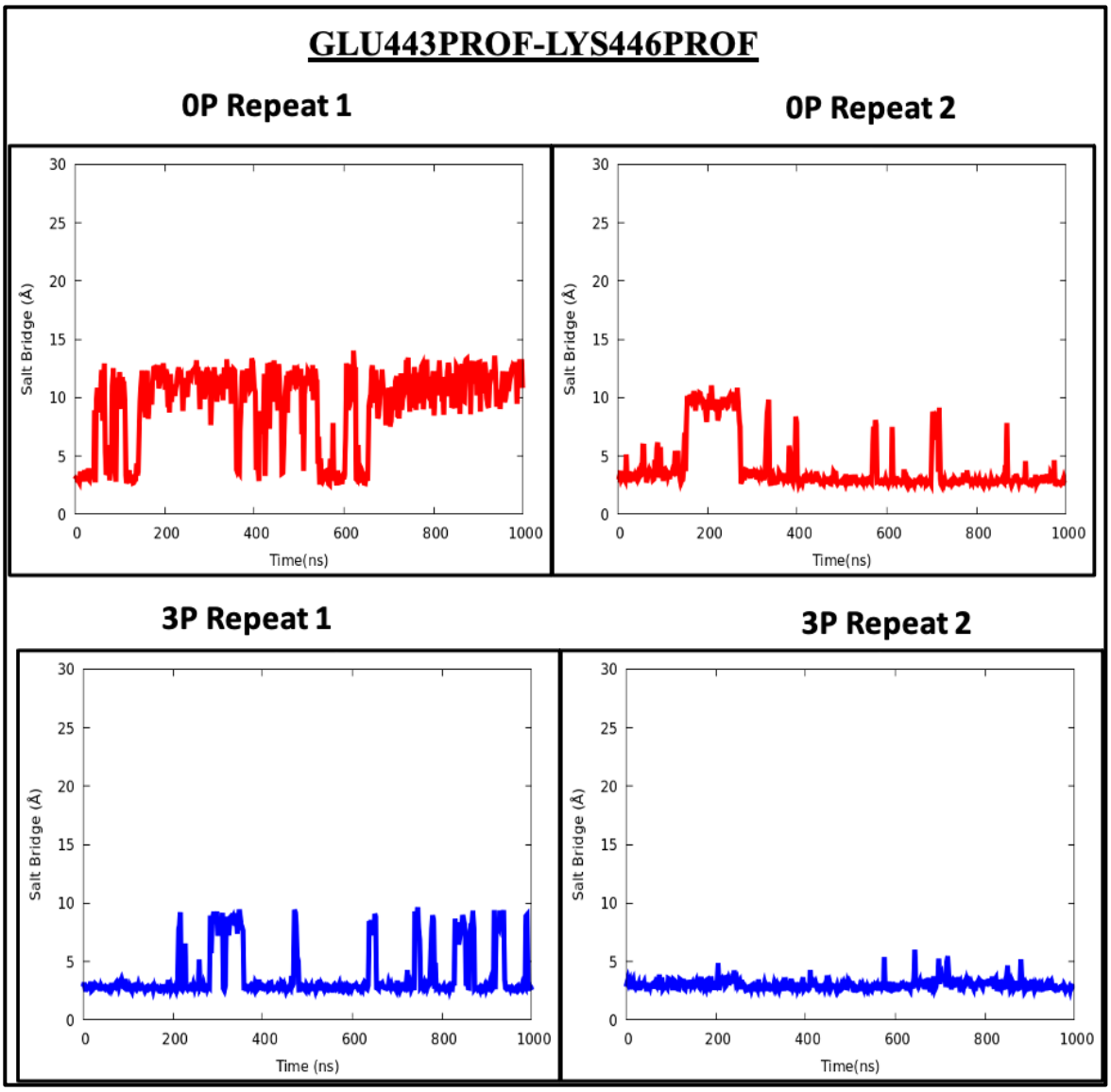

Figure 13. Salt Bridge dynamic between Glu443 on segment PROF and LYS446 on segment PROF over the 1000 nanosecond time frame is depicted above for 3P(blue) and 0P(red) systems.

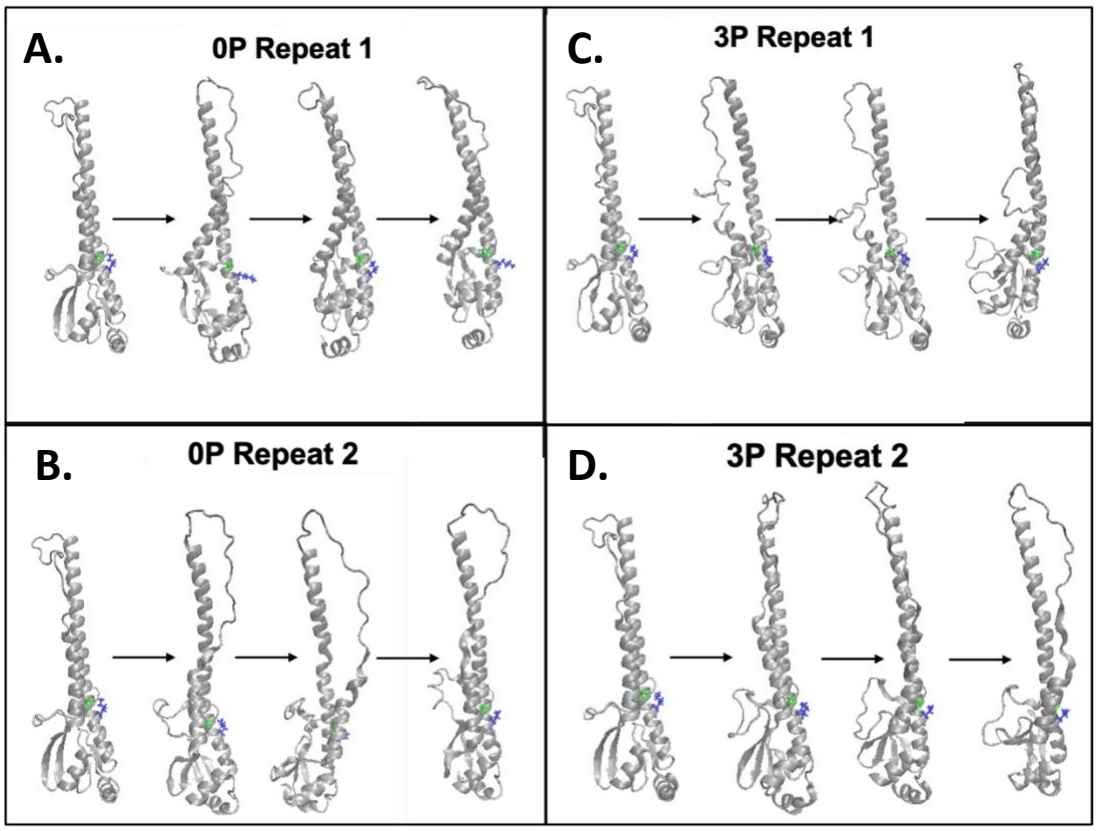

Figure 14. Glu443 (green residue) on segment PROF and LYS446(blue residue) on segment PROF are depicted above for all repeats. The leftmost visualizations occur at 0 us. The rightmost visualizations are the glycoproteins at 1 μs. Parts A and D each capture the middle segments after 300 ns and 600 ns, respectively. Parts B and C capture the middle segments after 312 ns and 520 ns, respectively.

At the start of the simulations, both 0P repeats exhibit a salt-bridge between Glu443PROF and Lys446 PROF. The salt bridge is broken in both 0P repeats before 200 ns. The salt bridge is on average more stable in the 3P repeats, as it is present during the majority of the 1000 ns time frame. The variation between the dynamic of this salt bridge in the segment can be attributed to the bending in the locale of the helical region containing the relevant residues. After 1000 ns, the salt bridge is broken in both in 0P-repeat 1 and 3P-repeat 1 as depicted in **Figure 13**. After visualization**(Figure 14)**, it appears the bending of the helical region containing the residues facilitates salt bridge formation by decreasing the distance between the residues, whereas the salt bridge breaks when the region straightens. The angular changes occurring in the region with the residues, result in salt bridge formation when the distance between the residues is decreased below 3.2 Å or breakage when it is increased past the 3.2 Å cutoff, increasing the

distance between the residues. The proximity of this salt bridge to the hinge histidine should also be noted

V. Conclusions and Future Work

The full scope of the expected HA2 mechanism was not captured within the one microsecond simulation period for each system. Previous preliminary models on the full Hemagglutinin structure spanned a 2.4 us period. Simulations are ongoing to encompass more of the configuration dynamic on HA2. All HA2 models exhibited distancing of their monomers at the C-terminus. All repeats exhibited localized dynamic conformational differences such as bending of alpha helices that contributed to the presence of different salt bridges across 0P and 3P repeats. A large-scale conformational change was not observed during the simulation period. Neither the expected helix to loop (at the hinge region) or loop to helix configuration were observed during the one microsecond simulation period.

Currently, there are no commercially available Influenza antivirals specific to the HA glycoprotein, which is why research in this area is beneficial.[2-3] An understanding of the pH-dependent configuration dynamic of HA2 through highly conserved residues allows for future research into standardized pharmaceuticals and drug therapies which are particularized to specific stages of HA activity and potentially have an all-encompassing applicability when it comes to targeting diverse influenza strains; Additionally, the structure and mechanism of the HA bears similarity to many other significant viral glycoproteins such as coronavirus spike proteins[11], indicating that further understanding the mechanism of HA can also provide insight into the workings of other notable proteins.

VI. References

1. Haldar, S., E. Mekhedov, C. D. McCormick, P. S. Blank, and J. Zimmerberg. 2019. Lipid-dependence of target membrane stability during influenza viral fusion. *Journal of* Cell Science. 132.
2. Jakubcova, L., M. Vozarova, J. Holly, K. Tomcikova, M. Fogelova, K. Polcicova, F. Kostolansky, E. Fodor, and E. Vareckova. 2019. Biological properties of influenza a virus mutants with amino acid substitutions in the ha2 glycoprotein of the ha1/ha2 interaction region. Journal of General Virology. 100:1282–1292.
3. Kalani, M. R., Moradi, A., Moradi, M., & Tajkhorshid, E. (2013). Characterizing a histidine switch controlling pH-dependent conformational changes of the influenza virus hemagglutinin. Biophysical journal, 105(4), 993–1003. https://doi.org/10.1016/j.bpj.2013.06.047
4. Trost, J. F., Wang, W., Liang, B., Galloway, S. E., Agbogu, E., Byrd-Leotis, L., & Steinhauer, D. A. (2019). A conserved histidine in Group-1 influenza subtype hemagglutinin proteins is essential for membrane fusion activity. Virology, 536, 78–90. https://doi.org/10.1016/j.virol.2019.08.005
5. Hu, B., C. T. Hofer, C. Thiele, and M. Veit. 2019. Cholesterol binding to the transmembrane region of a group 2 hemagglutinin (ha) of influenza virus is essential for virus replication, affecting both virus assembly and ha fusion activity. Journal of Virology. 93.
6. Anderson, R. G. W. and K. Jacobson. 2002. Cell biology - a role for lipid shells in targeting proteins to caveolae, rafts, and other lipid domains. Science. 296:1821–1825.
7. Eller, M. W., Siaw, H. M. H., & Dyer, R. B. (2021). Stability of HA2 Prefusion Structure and pH-Induced Conformational Changes in the HA2 Domain of H3N2 Hemagglutinin. Biochemistry, 60(35), 2623–2636. https://doi.org/10.1021/acs.biochem.1c00551
8. Strauch, E.M., Bernard, S.M., La, D., Bohn, A.J., Lee, P.S., Anderson, C.E., Nieusma, T., Holstein, C.A., Garcia, N.K., Hooper, K.A., Ravichandran, R., Nelson, J.W., Sheffler, W., Bloom, J.D., Lee, K.K., Ward, A.B., Yager, P., Fuller, D.H., Wilson, I.A., Baker, D. (2017) Nat Biotechnol **35**: 667-671

9. Madhusoodanan, M., & Lazaridis, T. (2003). Investigation of pathways for the low-pH conformational transition in influenza hemagglutinin. Biophysical journal, 84(3), 1926–1939. https://doi.org/10.1016/S0006-3495(03)75001-2
10. Superti, F., M. Agamennone, A. Pietrantoni, and M. G. Ammendolia. 2019. Bovine lactoferrin prevents influenza a virus infection by interfering with the fusogenic function of viral hemagglutinin. Viruses-Basel. 11.
11. Lang Y, Li W, Li Z, Koerhuis D, van den Burg ACS, Rozemuller E, Bosch BJ, van Kuppeveld FJM, Boons GJ, Huizinga EG, van der Schaar HM, de Groot RJ. Coronavirus hemagglutinin-esterase and spike proteins coevolve for functional balance and optimal virion avidity. Proc Natl Acad Sci U S A. 2020 Oct 13;117(41):25759-25770. doi: 10.1073/pnas.2006299117. Epub 2020 Sep 29. PMID: 32994342; PMCID: PMC7568303.
12. Caffrey, M., & Lavie, A. (2021). pH-Dependent Mechanisms of Influenza Infection Mediated by Hemagglutinin. Frontiers in molecular biosciences, 8, 777095. https://doi.org/10.3389/fmolb.2021.777095
13. Understanding the Stabilizing Effect of Histidine on mAb Aggregation: A Molecular Dynamics Study Suman Saurabh, Cavan Kalonia, Zongyi Li, Peter Hollowell, Thomas Waigh, Peixun Li, John Webster, John M. Seddon, Jian R. Lu, and Fernando Bresme Molecular Pharmaceutics 2022 19 (9), 3288-3303 DOI: 10.1021/acs.molpharmaceut.2c00453
14. S. Jo, T. Kim, V.G. Iyer, and W. Im (2008) CHARMM-GUI: A Web-based Graphical User Interface for CHARMM. J. Comput. Chem. 29:1859-1865
15. Ban, X., Lahiri, P., Dhoble, A. S., Li, D., Gu, Z., Li, C., Cheng, L., Hong, Y., Li, Z., & Kaustubh, B. (2019). Evolutionary Stability of Salt Bridges Hints Its Contribution to Stability of Proteins. Computational and structural biotechnology journal, 17, 895–903. https://doi.org/10.1016/j.csbj.2019.06.022
16. Bandyopadhyay, A. K., Ul Islam, R. N., & Hazra, N. (2020). Salt-bridges in the microenvironment of stable protein structures. Bioinformation, 16(11), 900–909. https://doi.org/10.6026/97320630016900

17. Pace, C. N., Fu, H., Lee Fryar, K., Landua, J., Trevino, S. R., Schell, D., Thurlkill, R. L., Imura, S., Scholtz, J. M., Gajiwala, K., Sevcik, J., Urbanikova, L., Myers, J. K., Takano, K., Hebert, E. J., Shirley, B. A., & Grimsley, G. R. (2014). Contribution of hydrogen bonds to protein stability. Protein science : a publication of the Protein Society, 23(5), 652–661. https://doi.org/10.1002/pro.2449
18. Brooks B.R., Bruccoleri R.E., Karplus M. CHARMM: a program for macromolecular energy, minimization, and dynamics calculations. J. Comput. Chem. 1983;4:187–217. [Google Scholar]
19. Brooks B.R., Brooks C.L., Karplus M. CHARMM: the biomolecular simulation program. J. Comput. Chem. 2009;30:1545–1614. [PMC free article] [PubMed] [Google Scholar]
20. Brooks, B. R., Brooks, C. L., 3rd, Mackerell, A. D., Jr, Nilsson, L., Petrella, R. J., Roux, B., Won, Y., Archontis, G., Bartels, C., Boresch, S., Caflisch, A., Caves, L., Cui, Q., Dinner, A. R., Feig, M., Fischer, S., Gao, J., Hodoscek, M., Im, W., Kuczera, K., … Karplus, M. (2009). CHARMM: the biomolecular simulation program. Journal of computational chemistry, 30(10), 1545–1614. https://doi.org/10.1002/jcc.21287
21. Armstrong, R. T., A. S. Kushnir, and J. M. White. 2000. The transmembrane domain of influenza hemag- glutinin exhibits a stringent length requirement to support the hemifusion to fusion transition. Journal of Cell Biology. 151:425–437.
22. Carr, C. M. and P. S. Kim. 1993. A spring-loaded mechanism for the conformational change of influenza hemagglutinin. Cell. 73:823–832.
23. Bullough, P. A., F. M. Hughson, J. J. Skehel, and D. C. Wiley. 1994. Structure of influenza hemagglutinin at the ph of membrane-fusion. Nature. 371:37–43.
24. Yates, Z., Gunasekaran, K., Zhou, H., Hu, Z., Liu, Z., Ketchem, R. R., & Yan, B. (2010). Histidine residue mediates radical-induced hinge cleavage of human IgG1. The Journal of biological chemistry, 285(24), 18662–18671. https://doi.org/10.1074/jbc.M110.108597
25. J. Lee, X. Cheng, J.M. Swails, M.S. Yeom, P.K. Eastman, J.A. Lemkul, S. Wei, J. Buckner, J.C. Jeong, Y. Qi, S. Jo, V.S. Pande, D.A. Case, C.L. Brooks III, A.D. MacKerell Jr, J.B. Klauda, and W. Im (2016)
CHARMM-GUI Input Generator for NAMD, GROMACS, AMBER, OpenMM, and

CHARMM/OpenMM Simulations using the CHARMM36 Additive Force Field. J. Chem. Theory Comput. 12:405-413

26. Texas Advanced Computing Center (TACC) The University of Texas at Austin